AMERICAN JOURNAL OF PHYSIOLOGY
GASTROINTESTINAL AND LIVER PHYSIOLOGY

Am J Physiol Gastrointest Liver Physiol 328: G545–G557, 2025.
First published April 7, 2025; doi:10.1152/ajpgi.00330.2024

RESEARCH ARTICLE

Optogenetic activation of the gut-brain axis in freely moving mice using a fully implantable wireless battery-free device

Timothy J. Hibberd,[1]* Andrew Efimov,[2,3]* Yue Wang,[2,3] Mingzheng Wu,[2] Lee Travis,[1] Kaila Ting,[2,4] Min-Kyu Lee,[2] Joohee Kim,[2,5] Jiheon Kang,[2] Mohammad Riahi,[6] Melinda Kyloh,[1] Vladimir Zagorodnyuk,[1] Hongzhen Hu,[7,8,9] John A. Rogers,[2,3,10,11,12] Nick J. Spencer,[1] and Abraham Vázquez-Guardado[6,13]

[1]*College of Medicine and Public Health, Flinders Health and Medical Research Institute, Flinders University, Adelaide, South Australia, Australia;* [2]*Querrey Simpson Institute for Bioelectronics, Northwestern University, Evanston, Illinois, United States;* [3]*Department of Biomedical Engineering, Northwestern University, Evanston, Illinois, United States;* [4]*Department of Neuroscience, Northwestern University, Evanston, Illinois, United States;* [5]*Center for Bionics of Biomedical Research Division, Korea Institute of Science and Technology, Seoul, Republic of Korea;* [6]*Department of Electrical and Computer Engineering, North Carolina State University, Raleigh, North Carolina, United States;* [7]*The Kimberly and Eric J. Waldman Department of Dermatology, Icahn School of Medicine at Mount Sinai, New York, New York, United States;* [8]*The Nash Family Department of Neuroscience, Icahn School of Medicine at Mount Sinai, New York, New York, United States;* [9]*Mark Lebwohl Center for Neuroinflammation and Sensation, Icahn School of Medicine at Mount Sinai, New York, New York, United States;* [10]*Department of Materials Science and Engineering, Northwestern University, Evanston, Illinois, United States;* [11]*Department of Neurological Surgery, Feinberg School of Medicine, Northwestern University, Chicago, Illinois, United States;* [12]*Center for Bio-Integrated Electronics, Northwestern University, Evanston, Illinois, United States; and* [13]*Center for Advanced Self-Powered Systems of Integrated Sensors and Technologies (ASSIST), North Carolina State University, Raleigh, North Carolina, United States*

Abstract

Considerable evidence suggests that the gut-brain axis can influence behavior. However, there has been a conspicuous lack of technology to provide targeted wireless activation of the gut-brain axis in conscious freely moving animals. We utilized a miniature fully implantable battery-free device to apply highly controlled optogenetic stimuli to the terminal region of gastrointestinal tract, in conscious freely moving mice. The optical stimulator was implanted and secured on the serosal surface of the distal colon and rectum to characterize the behavioral responses evoked by optogenetic stimulation of axons expressing channelrhodopsin (ChR2) driven by the Trpv1 promoter (Trpv1^{Cre+}ChR2 mice). In freely moving Trpv1^{Cre+}ChR2 mice, trains of blue light pulses to the distal colon and rectum induced increased abdominal grooming and reduced movement. In contrast to stimulation of the gut, trains of stimuli applied to the peritoneal cavity evoked writhing and abdominal contraction. Anterograde labeling from nodose ganglia revealed sparse vagal afferent axons and endings in the proximal and mid colon, with no labeled axons caudal of the mid colon (within 30 mm of the anus). The distal colon and rectum were densely innervated by spinal afferents. The findings demonstrate that wireless optogenetic stimulation of the gut-brain axis can induce specific behavioral patterns in conscious freely moving rodents, using fully implantable battery-free technology.

NEW & NOTEWORTHY The findings demonstrate that distinct behavioral changes can be induced by wireless activation of the terminal region of the large intestine (distal colon and rectum) in freely moving rodents, using fully implantable battery-free devices.

battery-free optical stimulator; enteric nervous system; gut-brain axis; implantable wireless devices; optogenetics

INTRODUCTION

Increasing evidence suggests that communication between the gut and brain plays an important role in health and well-being (1–3). However, developing technology that can be used to apply targeted stimulation of specific regions of gastrointestinal tract (GI tract) has been difficult to address in conscious free-to-move animals.

*T. J. Hibberd and A. Efimov contributed equally to this work.
Correspondence: A. Vázquez-Guardado (abraham.vg@ncsu.edu); N. J. Spencer (nicholas.spencer@flinders.edu.au); J. A. Rogers (jrogers@northwestern.edu).
Submitted 18 October 2024 / Revised 15 December 2024 / Accepted 2 April 2025

Spinal and vagal afferent neurons represent the two major sensory nerves that detect and relay sensory stimuli from the gastrointestinal tract (GI tract) to the brain (4–9). More is known about the functional role of vagal afferents because of the comparative ease of accessing and studying vagal afferent neurons in vivo. Behavioral changes induced by the activation of vagal afferents are generally believed to underlie affective aspects of visceral pain, like nausea, fear, and anxiety (10–12). In contrast, the less studied spinal afferent neurons in vivo have traditionally been considered to encode largely, or exclusively, painful (noxious) signals, whose behavioral responses are associated with reduced movement, hunched posture, vocalization, writhing, and abdominal contractions (4, 11, 13). However, recent emerging data show that spinal afferents that project to the gut relay a variety of sensory signals, far greater than simply noxious stimuli along the gut-brain axis, including monitoring of food intake (14), glucose homeostasis (15), and serotonergic signaling underlying anxiety (16).

Much of our understanding of the mechanisms underlying visceral sensation from the GI tract has involved studies of anesthetized animals (17, 18), or conscious animals that are physically restrained, such as during recordings of the visceromotor response (VMR) evoked by colonic distension (13, 19–22). Hence, a major weakness in the field is a lack of understanding of behavioral changes induced by selective activation of discrete regions along the GI tract in conscious unrestrained animals.

Here, we utilized a recently developed fully implantable optogenetic device that allowed highly controlled delivery of optical stimuli to the distal colon and rectum in conscious untethered mice (23). We identify distinct behavioral responses induced by stimulation of the gut-brain axis from the terminal gut that were vastly different from responses evoked by the same stimuli applied to the peritoneal cavity. These findings demonstrate that wireless optogenetic technology can be used to understand complex behavioral changes induced by optical stimulation of visceral pathways in unrestrained animals.

MATERIALS AND METHODS

Declaration of Ethics

Surgical procedures were approved by the Animal Welfare Committee of Flinders University (Ethics Approval Nos. 4004 and 3999), and all protocols carried out in accordance with the National Health and Medical Research Council (NHMRC) *Australian code for the care and use of animals for scientific purposes* (8th edition, 2013) and recommendations from the NHMRC *Guidelines to promote the wellbeing of animals used for scientific purposes* (2008). We support inclusive, diverse, and equitable conduct of research.

Experimental Model and Study Participant Details

Homozygous Trpv1 cre ($Trpv1^{Cre+}$) mice were kindly donated by Prof. Brett Graham at the University of Newcastle and crossbred with Rosa-CAG-LSL-ChR2(H134R)-eYFP-WPRE (Ai32) homozygous mice. Resulting $Trpv1^{Cre+}$ ChR2 mice expressed the light-sensitive cation channel, Channelrhodopsin-2 (ChR2), and the enhanced yellow fluorescent protein reporter (eYFP) in $Trpv1^{+}$ neurons. Mice of either sex, from 2 to 6 mo old, were housed in the Flinders Medical Centre Animal Facility, under a 12-h light/dark cycle with food and water provided ad libitum. Control groups consisted of two variants, one where C57BL/6 mice lacking ChR2 expression (biological control) were implanted with wireless devices that drive the array of blue light-emitting diodes (LEDs). The other type of control we tested involved $Trpv1^{Cre+}$ ChR2 mice implanted with wireless devices with inoperable LEDs (surgical control or sham).

Hard-Wired LED Stimulation on Anesthetized Animals

Blue light-emitting diodes (LEDs; model number CREE C479 DA2432) were purchased from Three Five (III-V) Materials, Inc., New York, NY. Each LED was soldered to the miniature flexible printed circuit board (fPCB; PCBWay, Hangzhou, Zhejiang, PR China) and attached to 20-mm-long enameled copper wire, coated in light-cure acrylic (Loctite 3554) and polydimethylsiloxane elastomer (PDMS, Sylgard 184, Dow). A custom-made wired LED driver box (Flinders Biomedical Engineering; BME1627) with a 0- to 15-V direct current power supply was used to manually set the operational voltage of the LEDs. They were connected at a four-position terminal block at the front of the box along with a voltmeter and a wire jumper. Power to the LEDs was triggered using the 10-V analog output from a PowerLab 16/35 (ADInstruments, Bella Vista, Australia). Stimulus parameters including pulse width, frequency, and train duration were set and triggered using LabChart 7 software (ADInstruments). The optical power intensity in mW/mm^2 versus voltage was characterized for each LED used. Activation thresholds were tested on tissue, and the maximum intensity was used for experimental stimulations.

Fabrication of the Wireless Battery-Free Device for In Vivo Optogenetic Rectal Afferents

Custom-made wireless battery-free devices were modified from a recent study (23–25). The optogenetic stimulator consisted of three LEDs mounted on a paddle-like probe that provided sufficient length for implantation under the pelvic bone to access the rectal wall. This configuration allowed for optogenetic stimulation of the terminal rectum <5 mm from the anal sphincter, a region that is normally inaccessible as a survival surgery. The wireless optogenetic device comprised two modules: the main circuit board that contained the wireless control and power harvesting, and the paddle-like probe that held the three LEDs. These parts were customized flexible printed circuit boards (fPCBs) outsourced to third-party vendors (PCBWay, Hangzhou, Zhejiang, PR China). Both fPCBs consisted of double-sided copper (18 μm) traces on polyimide (PI, 25 μm) substrate; however, the main board was covered with an additional PI cover lay (12.5 μm) on both sides, whereas the paddle was not, to reduce mechanical stiffness. Following the electronic component soldering, tinsel wires (type 1#, Round Teck Intl. Co.) were soldered on through-hole connections at both ends for added strength. Three blue LEDs (1 mm × 1 mm, 450 nm, Cree SA1000) were soldered to the paddle. Norland UV curable adhesive 61 (NOA61) was applied over the components and exposed solder joint regions of the printed circuit board (PCB) and cured to strengthen the main circuit board to the LED paddle connection. Conformal coating of parylene-C (10 μm) coated the devices to provide electrical insulation. A layer of PDMS was

applied on both sides of the two PCBs to create a softer interface between the device and surrounding tissue. Finally, Kwik-Sil silicone sealant was placed around the solder joints to further insulate the wires and reduce bending fatigue.

Wireless Power Transfer and Remote Control of the Implanted Devices

A circular polyvinyl chloride (wall thickness 1.7 mm) with an inner diameter of 15.5 cm, wrapped with two loops of multistrand cable (American Wire Gauge, AWG 16), was used to create the magnetic cavity. The lower loop was positioned at a height of 25 mm from the base, and the second loop at a height of 60 mm from the base. The multistrand cable comprised 30 wires of 0.25 mm diameter, which resulted in an equivalent of 1.47 mm^2. The commercial radio frequency (RF) power distribution and control box (PDC Box, Neurolux) supplied constant power at 13.56 MHz to power up the implanted device via magnetic induction. The use of this RF system, equipped with near-field communication (NFC) capability, provided bidirectional communication between a homemade graphic user interface (GUI, MATLAB, The MathWorks, Inc.) and the implanted devices. Here, the PDC Box communicated with the implanted device using the ISO 15693 NFC protocol, supported in an RF-accessible random-access memory on the device (M24LR04E, STMicroelectronics). This implementation permitted the interchange of commands with the device such as start/stop, LED sequence selection, and operation parameter update such as frequency, pulse width, and LED sequence, interpreted and executed on a low-power microcontroller (Attiny84, Atmel). In this way, the user had full control of the device and its operation once implanted (23, 24).

Definitions of Anatomy in Mouse Large Intestine

In this study, the rectum is defined as the region caudal of the pelvic bone, that is, the region innervated by rectal nerves. This occupies ~15 mm from the anal sphincter in an unstretched, intact, whole large intestine. The distal colon is defined as the region within 10 mm rostral of the pelvic bone. This is the area of large intestine that is visible during laparotomy. The LED paddle was implanted under the pelvic bone in the terminal rectum, which involves a region <5 mm from the anal sphincter.

Immunohistochemistry

Lumbosacral dorsal root ganglia (DRG) were removed from euthanized $Trpv1^{Cre+}$ChR2 mice and fixed in 4% paraformaldehyde for ~12 h, then washed in phosphate buffer solution (PBS). DRG were then immersed in 0.5% triton in PBS and blocked with 10% normal horse serum (NHS; Life Technologies Gibco, Cat. No. 16050-122; Scoresby, Australia) in antibody diluent, before incubation for 48 h in 1:2,000 guinea pig anti-Trpv1 antibodies (Alomone Labs, Cat. No. ACC-030-GP, formerly AGP-118) and 1:1,000 rabbit anti-green fluorescent protein (GFP) antibodies (Thermo Fisher, Cat. No. A-11122). The tissue was then incubated in 1:200 Cy5 donkey anti-guinea pig and 1:200 fluorescein isothiocyanate (FITC) donkey anti-rabbit in antibody diluent for 12 h before final washing in PBS and mounted on microscopy slides with 100% glycerol.

For calcitonin gene-related peptide (CGRP) immunolabeling, wholemount preparations of colon and rectum were fixed overnight in 4% paraformaldehyde (in PBS; pH 7.2). Mucosa was removed by sharp dissection, cleared with dimethyl sulfoxide, and then blocked for 1 h with 10% NHS in antibody diluent. Preparations were then incubated in primary antibody (rabbit anti-CGRP; 1:2,000 dilution from neat antiserum in 10% NHS; Peninsula Laboratories International Inc., Cat. No. T-4032; San Carlos, CA) for 2 days. Finally, preparations were incubated in secondary antibody (donkey anti-rabbit Cy3; 7.5 μg/mL; Jackson ImmunoResearch Laboratories Inc., Cat. No. 711-165-152; West Grove, PA) for 4 h, before mounting the serosal side uppermost on glass slides in 100% carbonate-buffered glycerol (pH 8.6). All antibodies and block solutions were diluted with PBS containing 0.1% sodium azide, and PBS washes were performed between all antibody incubation steps.

Surgical Implantation of Wireless Devices In Vivo

$Trpv1^{Cre+}$ChR2 mice of either sex were anesthetized with isoflurane, induced at 4%, and then maintained at 1.5%–2% in 1 L/min oxygen. Depth of anesthesia was monitored by lack of response to a hind limb or tail pinch. Mice were positioned on a thermostat-controlled heat mat to maintain body temperature (Adloheat, Pakenham, VIC, Australia). Before incision, animals were administered subcutaneously 0.05 mg/kg buprenorphine (Temvet). The dorsal surface was shaved and cleaned with 0.5% chlorhexidine and 70% alcohol swab (Briemar). A laparotomy was performed, and the LED paddle was positioned under the pelvic bone with LEDs facing the rectum. The device's wireless receiver was positioned subcutaneously in the lower abdomen, proximal to the LED paddle, with wiring fed through the abdominal muscle. Post recording, mice were euthanized and the LED position relative to the rectum was inspected to verify its location.

Retrograde Tracing from the Large Intestine

For retrograde tracing using 1,1′-didodecyl-3,3,3,3′-tetramethylindocarbocyanine perchlorate (DiI, C12 version), $Trpv1^{Cre+}$ChR2 mice (of either sex) expressing the enhanced yellow fluorescent protein reporter (eYFP) in $Trpv1^{+}$ neurons were used. These mice were prepared for surgery as described for implantation earlier. After midline laparotomy, DiI was injected into the distal colon (adjacent to the pelvic bone) (~20 μm diameter) using a fine glass micropipette to penetrate the serosal surface. A custom-made spritz system was used to deliver pressure to the micropipette, as used previously to inject dorsal root ganglia (26). A single injection of DiI was made into the musculature with a total injection volume of ~1 μL. A fine layer of gauze was used to wrap underneath the distal colon to minimize any leakage of DiI. Mice were allowed to recover for a period of 7–12 days following dye injections, at which point mice were euthanized and lumbosacral DRGs removed. Following euthanasia, the abdominal viscera were inspected for leakage of DiI. Any preparations showing potential spread or leakage of DiI were discarded from the analysis. Nodose ganglia, DRG, and the whole colon and rectum were removed from animals. In a second cohort of animals, retrograde tracing using the identical protocol described earlier, cholera toxin subunit B fluorescent tracer (CTB-488) was used, again using single

injections using fine glass micropipettes and ~1 μL injection volumes.

Anterograde Labeling from Nodose Ganglia

The extent of vagal afferent innervation along the large intestine was investigated using anterograde tracing from nodose ganglia in vivo. The same anesthesia protocol was used for anterograde tracing experiments as with retrograde tracing described earlier. C57BL/6J mice of either sex (3–6 mo of age) were anesthetized and a 1–2 cm incision was made at the ventral surface of the neck to expose the right nodose ganglion, which was injected with 50–100 nL biotinylated dextran-biotin (20% in saline; Molecular Probes, Cat. No. D1956, RRID: AB_2307337) through a fine glass microelectrode, using a custom-made nitrogen-delivered drug spritzer system (Biomedical Engineering, Flinders University). Following injections of the tracer, the skin was sutured with 2.0 suture (Dynek, Australia). Mice were given a 7-day recovery period to allow for the tracer to be transported from the nodose ganglion to nerve terminals in the large intestine.

Visceromotor Responses in Anesthetized Mice

Visceromotor responses (VMRs) were elicited by electrical stimulation of the rectum during anesthesia with pentobarbital sodium (200–300 μL of 6 mg/mL, ~40–60 mg/kg). Depth of anesthesia was assessed by lack of response to the hind limb or tail pinch. Electromyographic electrodes were implanted into the left external oblique muscle and a reference electrode was placed in the quadriceps muscle of the opposing leg. Electromyography (EMG) recordings were acquired at 20 kHz on a PC running LabChart 7 Pro software and high-pass filtered (100 Hz). Analysis of EMG to compare the latency and efficacy of optical and electrical stimuli was also performed using LabChart 7 Pro (ADInstruments, Australia). A pair of stainless steel stimulating electrodes insulated to within ~2 mm of the tip was inserted into the rectum of mice for rectal stimulations (measured <5 mm from anal sphincter). Square single-pulse electrical stimuli were generated using a Grass SD9 stimulator unit (60 V, 0.5-ms pulse width). Following experiments, mice were euthanized by an overdose of pentobarbital sodium. All steps were taken to minimize subjective bias in the study design.

Image Capture and Fluorescence Microscopy

Whole mount DRG and preparations of large intestine were viewed using a fluorescence microscope (IX71; Olympus) with filters for FITC, Cy3, and Cy5 fluorophores (Chroma Technology) via Å~20 objective water-immersion lens. A Roper Scientific (CoolSNAP) camera along with AnalySIS Imager 5.0 (SIS; Olympus, Münster, Germany) was used for image capture. Quantification of the eYFP marker (enhanced by GFP immunofluorescence) and Trpv1^{+} immunofluorescence in retrogradely labeled spinal afferent nerve cell bodies was performed by overlaying images of DRG from the three different fluorophore filters using ImageJ (v1.53a, NIH).

Wireless Stimulation Protocols

Mice were allowed a 3-day recovery after device implantation and placed in the wireless cavity (chamber) for a 12-min-long recording period, which consisted first of 4 min of baseline (no stimulation), then 4 min of optogenetic stimulation was applied, followed by 4-min recovery (off stimulation) period. The 4-min stimulation period consisted of continuous stimulation with pulses of blue light 450 nm, 20 Hz, 10-ms pulse widths with 10 W RF applied to the cavity. This recording was made on the animal's first encounter with the recording chamber, which was undertaken to limit habituation variability that could be caused by repetitive exposure to the chamber. A second, "phasic" stimulus protocol was employed, which was identical to the first protocol, except that phasic pulses of light were applied consisting of 20 s on, followed by 40 s off each minute, for 4 min. As mentioned for animals, two types of control groups were tested for behavioral experiments: Trpv1^{Cre+}ChR2 mice, rectally implanted with wireless devices containing inoperable LEDs (sham, $n = 5$), and C57Bl/6J mice rectally implanted with wireless devices containing active LEDs (biological controls, $n = 5$). Because no statistical differences between the two types of control were observed, we aggregated both types forming a single control group containing surgical and biological controls in equal numbers.

Quantification and Statistical Analysis

Results are expressed as means ± SD unless otherwise indicated, with n referring to the number of animals on which observations were made. Statistical analysis was done using Prism v.10 software (GraphPad Software, Inc., San Diego, CA). For assumption checking, the Shapiro–Wilk test was used to assess normality, and homoscedasticity plots were assessed visually. Nonparametric tests were used where data and log-transformed data failed to meet assumptions of normality and homoscedasticity. Details of statistical tests used are in the text. Differences were considered significant if $P < 0.05$.

RESULTS

Implantable Wireless Battery-Free Optogenetic Device

The stimulation of soft tissue in untethered freely moving mice represents a technological challenge. Here we used the recently developed implantable wireless, battery-free device, designed to address overarching challenges in optical power restrictions, remote control capability, and mechanical compliance required for applications in vivo (Fig. 1*A*) (23–25). This flexible electronic device consists of two functional components: *1*) the electronic base (11 mm × 14.75 mm, ~1 mm maximum thickness) that contains the communication, power management, and control; and *2*) a flexible paddle-like probe (13.1 mm × 1.4 mm) that contains the array of three blue LEDs (~1 mm^2 each, 450 nm), both connected using 0.22 mm diameter, 15-mm-long flexible tinsel wires (Fig. 1*D*). See MATERIALS AND METHODS for more fabrication details. A low-power microcontroller, continuously powered via RF wireless power transfer at 13.56 MHz, controls operation of the LEDs such as start and stop, and their temporal parameters such as frequency, pulse width, and sequence. The use of an NFC memory chip serves as the wireless communication link and allows the remote control of the optogenetic stimulator parameters on demand using a GUI in MATLAB. Furthermore, the device includes an energy

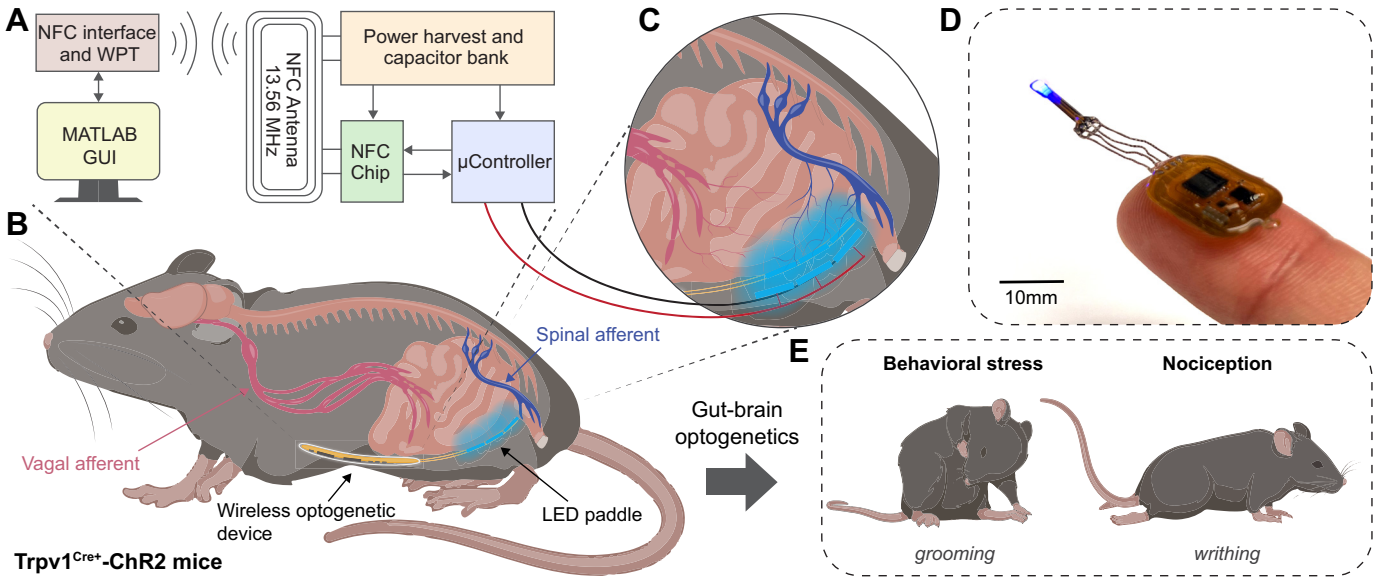

Figure 1. Implantable, wireless battery-free optogenetic device. *A*: block diagram that describes the remote operation of the wireless battery-free implantable device. The graphic user interface (GUI) encodes commands and configuration sent to the device wirelessly via near-field communication (NFC) using the radio frequency (RF) module operating at 13.56 MHz. The RF module also provides wireless power transfer (WPT) to the device. *B*: illustration of Trpv1^{Cre+}ChR2 mice with a subcutaneous wireless optogenetic device implanted in the lower abdomen. *C*: the three LED-mounted paddles positioned under the pelvic bone illuminate the terminal rectum (<5 mm from the anal sphincter). *D*: photograph of a device powered wirelessly that rests on a finger for size comparison. *E*: common behavioral outcomes expressed in mice during optogenetic stimulation of the spinal afferents in the rectum: grooming and writhing. ChR2, channelrhodopsin; LED, light-emitting diode.

storage module, in the form of a ceramic capacitor bank (1.72 mJ at 5.6 V), which drives pulses (~5 ms) of illumination at 7 mW/mm^2 (27). This illumination, in addition to the combined large area covered (~3 mm^2) and low risk of heat injury ($\Delta T < 1.1°C$), is strong to stimulate a large volume of colon tissue as compared with other similar battery-free implantable optogenetic devices (23). These operational capabilities, in addition to the lightweight (0.42 g) and fully implantable form factor, yield user-programmable wireless optogenetic stimulation and permit the observation of behavioral outcomes in cohorts of freely behaving mice (Fig. 1, *B*–*E*).

Identifying the Extent of Vagal Afferent Innervation along the Large Intestine

To determine the extent of vagal sensory innervation along the length of the large intestine, we performed in vivo anterograde tracing from nodose ganglia. Injection of dextran biotin unilaterally into the right nodose ganglion revealed sparse labeling of vagal afferent axons and nerve endings in 10 out of 24 mice (Fig. 2, *A* and *B*). In total, 31 single vagal axons were identified, which entered the proximal and mid colon via the mesentery (Fig. 2, *C* and *D*). Morphologically distinct nerve endings were identified, including intraganglionic lamellar endings. No vagal afferent axons or endings were identified caudal to the mid colon, that is, within 30 mm of the internal anal sphincter ($n = 10$, Fig. 2, *G* and *H*). To verify these observations, we performed retrograde labeling using a single injection of DiI (~1 µL) injected via fine glass micropipette into the distal colon (adjacent to the pelvic bone, ~20 mm from anal sphincter). We found dense labeling of nerve cell bodies in lumbosacral DRG (Supplemental Fig. S1), but not in nodose ganglia from four of five mice injected (Supplemental Fig. S1, $n = 5$). In one of the five mice injected with DiI into the distal colon, three faintly labeled nodose neurons were identified. Whether these represent spread of tracer from the injection site to vagal afferent terminals located more rostral in the proximal-mid colon was uncertain. To test this further using other retrograde tracers, we made single injections of the cholera toxin subunit B fluorescent tracer (CTB-488) into the same region of distal colon. Even when single injections of minute volumes of CTB (~1 µL) were made via fine glass microelectrodes, we obtained extensive nonspecific labeling of neurons in nodose ganglia. This was in part likely due to extensive uncontrolled spread of CTB throughout the full length of colon ($n = 3$). In this regard, we found retrograde tracing with CTB to be highly unreliable.

Prior to in vivo optogenetic experiments, we investigated the degree of expression of Trpv1 and eYFP in rectal-projecting spinal afferent neurons. To do this, the retrograde tracer DiI was injected into the distal colon adjacent to the pelvic bone (Fig. 3*A*). It was found that of all DiI-labeled nerve cell bodies in lumbosacral DRG, 74% (40/54 neurons) were GFP-immunoreactive (reflecting eYFP expression) and 32/54 (59%) were Trpv1-immunoreactive ($n = 5$). Importantly, 66% of GFP-immunoreactive DRG neurons were Trpv1-immunoreactive and 99% of Trvp1$^+$ neurons were GFP-immunoreactive (Fig. 3).

Comparison of Electrical versus Optical Activation of Rectal Afferents

We then investigated light activation of the gut-brain sensory pathway from the rectum in more detail in vivo. In anesthetized Trpv1^{Cre+}ChR2 mice, we sought to determine whether light was as effective as electrical stimulation in activating the afferent pathway from the rectum to the brain, by

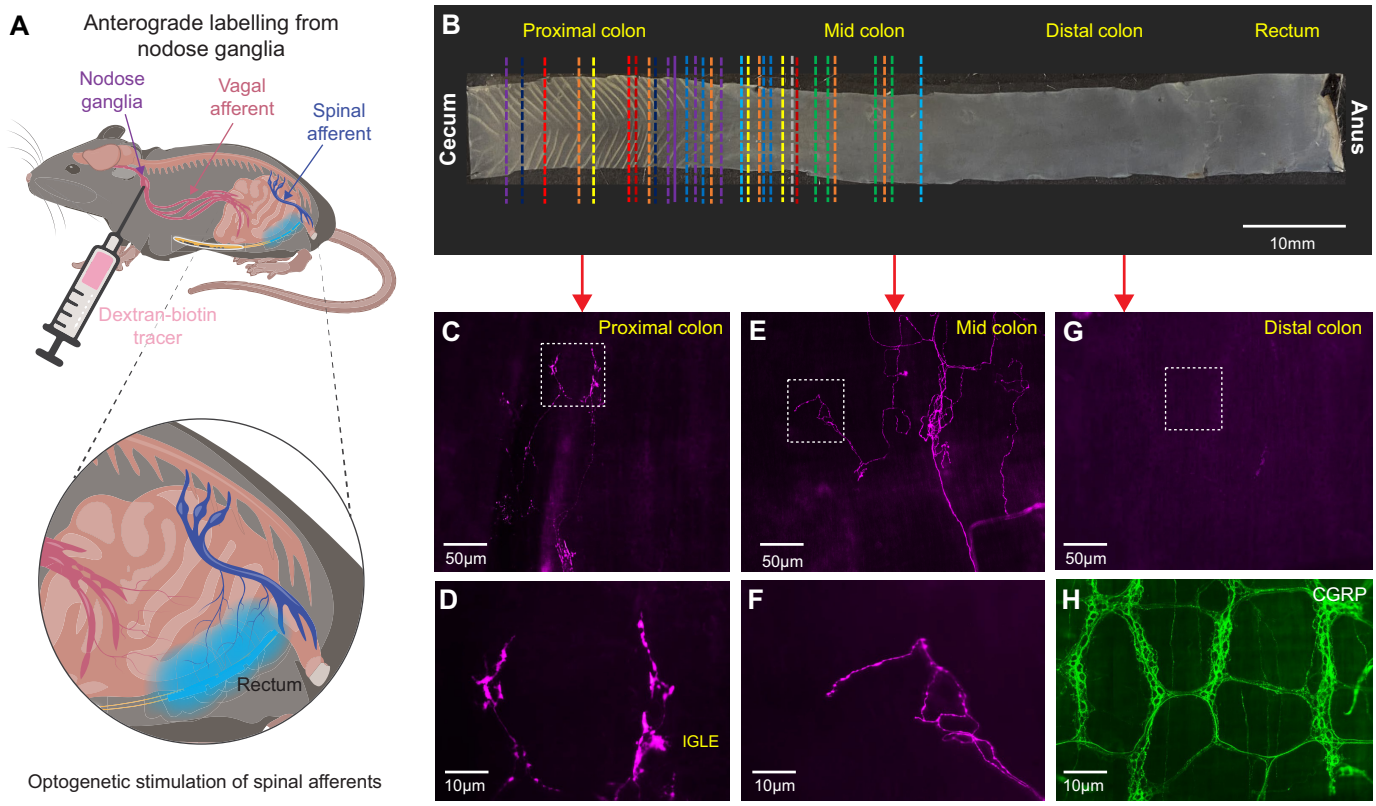

Figure 2. Anterograde tracing of vagal afferents to the colon. *A*: schematic of the injection site into nodose ganglia and sparse labeling of vagal afferent axons to the proximal and mid colon. Inset shows dense spinal afferents to the rectum, but absence of vagal afferents. Wireless LED placement in the rectum in vivo activates only spinal afferents to the rectum. *B*: photograph of whole isolated mouse colon. Each color represents a different mouse where vagal afferent labeling of single axons was revealed in the colon. Multiple lines of the same color represent more than one axon labeled within the same colon. In total, 31 vagal axons were identified from 10 mice. No vagal axons were identified in the region of large intestine (distal colon or rectum) that was within 30 mm of the anal sphincter. *C*: labeled vagal axon and endings in the proximal colon. *D*: magnified section of intraganglionic lamellar endings (IGLEs) as indicated by the white box in *C*. *E*: labeled varicose type vagal afferent axons in the mid colon. *F*: magnified section of varicose type vagal afferent endings as indicated by the white box in *E*. *G*: shows no labeling in distal colon. Region in the white box is shown on expanded scale in *H*. *H*: although the distal colon lacked vagal afferent labeling, there was dense CGRP immunoreactivity, consistent with an intact myenteric and spinal afferent nerve supply. CGRP, calcitonin gene-related peptide; LED, light-emitting diode.

quantifying changes in the VMR. To do this, we quantified VMR differences when blue light was applied by hard-wired LEDs to the rectum, compared against those evoked by electrical nerve stimuli to the same site (Fig. 4, *A* and *B*).

The effects of graded intensity (6–45 mW) of single light pulses applied to the rectal mucosa were compared against graded voltages (5–50 V) of single electrical pulse stimuli to the same region (Fig. 4, *C* and *D*). Increases in intensity of single blue light pulses increased the log of evoked spikes per pulse recorded from abdominal EMG ($P = 0.014$, simple linear regression, $n = 6$), but not the latency of spike onset (Fig. 4*C*), possibly reflecting changes in light penetration of the gut. Graded intensity single pulse electrical stimulations of the rectum showed no statistically significant relationship with the number of evoked spikes or latency (Fig. 4*D*).

Next, we compared EMG responses with trains of 10 optical or electrical pulses at frequencies ranging from 0.1 to 10 Hz. Although electrical stimulation evoked a relatively constant number of spikes across stimulation frequencies, optical stimulation showed a decline (fewer spikes per pulse) as frequency increased (Fig. 4*E*). The slopes of the electrical and optical stimulus-response profiles were significantly different ($P = 0.038$, simple linear regression, $n = 15$ total; optical stimulation = 15, electrical stimulation = 12; Fig. 4*F*), but not for the latency of EMG responses ($P = 0.837$, simple linear regression, $n = 15$ total; optical stimulation = 15, electrical stimulation = 13; Fig. 4, *G* and *H*). Thus, both optical and electrical pulses were followed by muscle action potentials with high fidelity at low stimulation frequencies, but this dropped off rapidly for optical stimulation as frequency increased. When EMG responses were normalized to time (spikes evoked per second), optical stimulation showed a relatively flat response profile compared with electrical stimulation, which showed a clear positive slope across the frequencies tested ($P < 0.0001$, linear regression, weighted least squares, $n = 15$ total; optical stimulation = 15, electrical stimulation = 12; Fig. 5, *A* and *B*), indicating a tendency for VMR magnitudes to optical but not electrical stimulation to "saturate" rapidly with increasing stimulus frequency. Consistent with this, the proportion of stimulations followed by muscle action potentials showed a decline with increasing frequencies (Fig. 5, *C* and *D*). Optical but not electrical stimulations had a negative slope, significantly different from zero ($P < 0.0001$ and $= 0.055$, respectively, simple linear regression, $n = 15$ total; optical stimulation = 15, electrical stimulation = 12; Fig. 5*D*). Comparison of the spike latency between

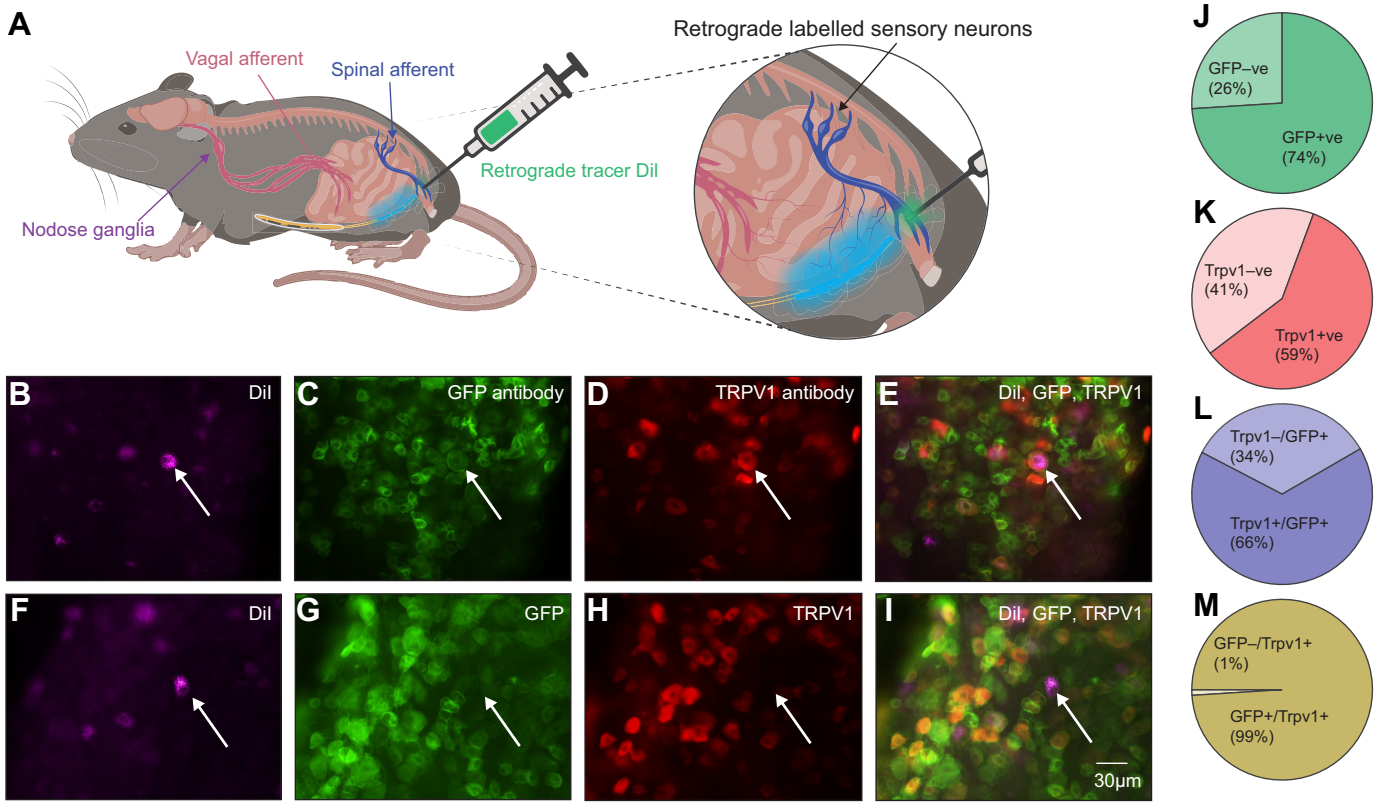

Figure 3. Retrograde tracing from the distal colon to dorsal root ganglia. *A*: illustration that shows the DiI retrograde labeling procedure from the rectal spinal afferents. *B*: DiI-labeled DRG nerve cell body retrogradely traced from the rectum. *C*: matched micrograph showing GFP immunoreactivity in the same cell body shown in *B* (arrow). *D*: Trpv1^{+} immunoreactivity. Arrow indicates the neuron shown in *B* and *C* is Trpv1^{+}. *E*: superimposed image of *B*–*D*. *F*: a retrogradely labeled DRG neuron that projects to the large intestine. *G*: matched micrograph to *F*, showing the neuron is not GFP-immunoreactive (arrow). *H*: Trpv1 immunoreactivity. Arrow indicates the neuron in *F* is not Trvp1^{+}. *I*: superimposed image of *F*–*H*. DiI was visualized with a Cy3 filter, GFP with FITC, Trpv1^{+} with Cy5. *J*–*M*: relative proportions of neurons that were GFP-immunoreactive, with accompanying Trpv1 immunoreactivity. DiI, 1,1′-didodecyl-3,3,3,3′-tetramethylindocarbocyanine perchlorate; DRG, dorsal root ganglia; FITC, fluorescein isothiocyanate; GFP, green fluorescent protein.

optical and electrical nerve stimulation, irrespective of frequency, revealed that the log of time between suprathreshold stimuli and muscle action potentials was consistently less for electrical stimulation compared with optical stimulation ($P = 0.001$, paired t test, $t = 4.256$, df $= 12$, $n = 13$; Fig. 5*E*). This may reflect the additional recruitment of faster-conducting fibers by electrical stimulation. We also compared the number of spikes elicited per stimulus pulse. The number of spikes within bursts of firing that regularly followed stimulation was quantified. Electrical stimulation always evoked more spikes than optical stimulation ($P = 0.005$, paired t test, $t = 3.539$, df $= 10$, $n = 11$; Fig. 5*F*). This may reflect the more selective recruitment of (Trpv1^{+}) fibers by optical stimulation.

Wireless Optogenetic Stimulation of the Rectum in Conscious Animals

To selectively stimulate the gut-brain pathway from the rectum in vivo, the LED paddle in the wireless devices was placed under the pelvic bone of Trpv1^{Cre+}ChR2 mice, opposing the rectal wall (Supplemental Fig. S2) and beyond the extent of vagal afferent innervation. A continuous 4-min stimulation protocol was used (20% duty cycle, 20 Hz, 10 ms pulses, 10 W power) and compared with 4-min quiescent baseline periods pre- and poststimulation. Compared with prestimulation baseline, this stimulus induced a significant increase in episodes of abdominal grooming, from 0.8 ± 0.9 episodes during baseline, to 7.3 ± 3.0 episodes during the stimulation period [$P = 0.010$, Dunn's posttest (stimulation vs. prestimulation control period), repeated measures Friedman test, Friedman statistic = 9.36, $P = 0.005$, $n = 7$, rectal stimulation group; see Fig. 6, *A* and *B*, and Supplemental Video S1]. Total duration of abdominal grooming episodes was also significantly increased during stimulation, but not in control animals [$P = 0.002$, Dunn's posttest (stimulation vs. prestimulation control period), repeated measures Friedman test, Friedman statistic = 11.63, $P < 0.001$, $n = 7$, rectal stimulation group; Fig. 6*C*]. Optogenetic stimulation of rectal afferents did not increase the number of episodes of nose, ear, or back grooming ($n = 7$; Supplemental Fig. S3). However, voluntary movements were significantly reduced [$P = 0.012$, Dunnett's posttest, two-way repeated measures ANOVA, main effect of group (rectal stimulation) $P = 0.001$, $F(1.44, 28.82) = 10.78$, $n = 7$, rectal stimulation group; see Fig. 7, *A* and *B*]. A similar reduction in movement was not detected in the control mice ($n = 10$, Fig. 7, *B* and *F*).

In the same mice, a phasic stimulation protocol was tested (4 min, at 20 Hz, 10 ms pulses). Phasic stimulation comprised cycling between a 20 s stimulus train (20% duty cycle; 10 ms pulse width, 20 Hz) followed by 40 s quiescence. Thus, a 4 min phasic stimulation period comprised

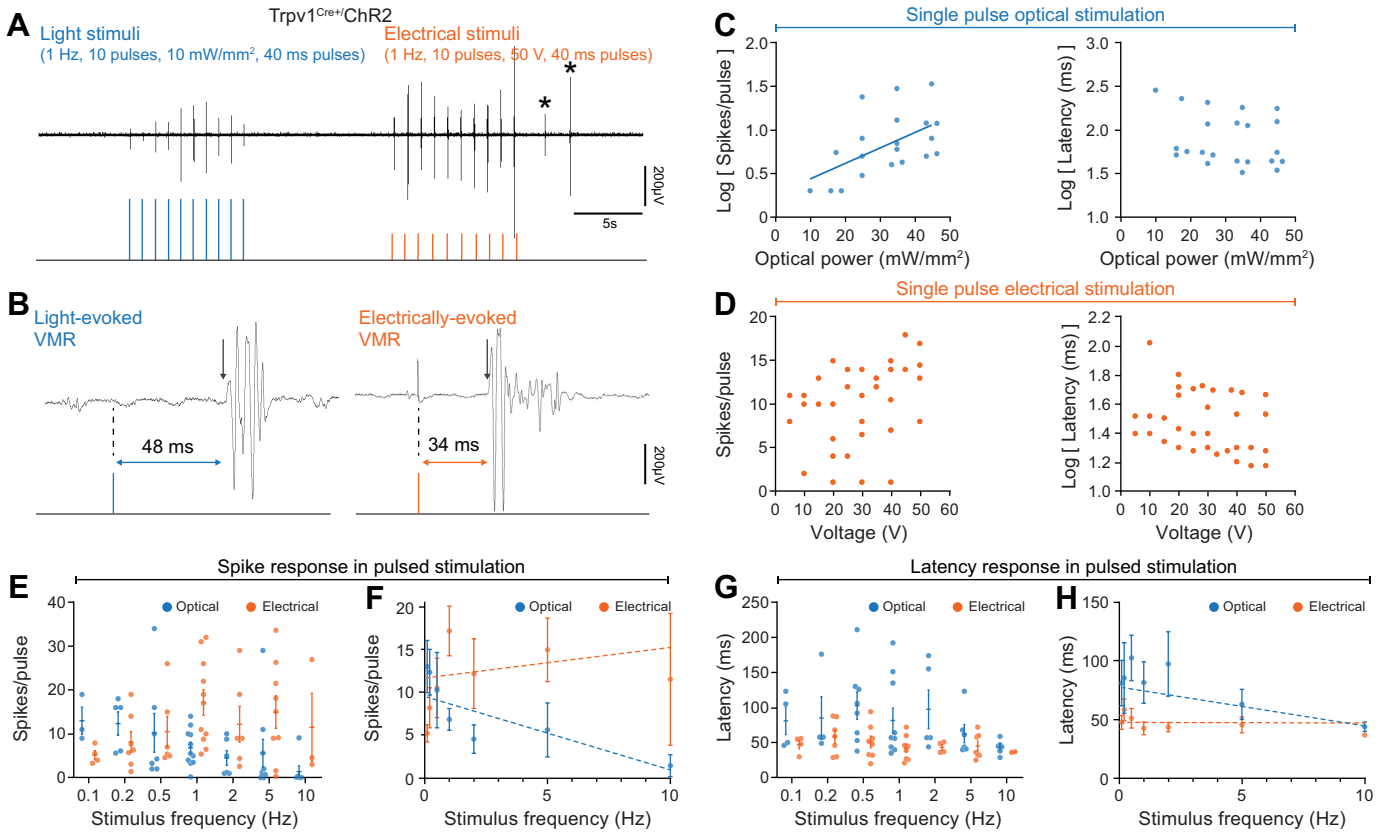

Figure 4. Characterization of EMG-recorded muscle action potentials evoked by rectal stimulation in anesthetized Trpv1^{Cre+}ChR2 mice. *A*: VMR recording showing single optical pulses to the rectum, followed by single electrical nerve stimuli at the same site. *Responses to tail pinch and hind limb pinches. *B*: expanded single light-evoked VMR with latency indicated, followed by electrically evoked VMR. *C*: graphs showing the number of evoked spikes and spike latency following single optical pulses across a range of optical powers. *D*: evoked spikes and spike latency across a range of single electrical pulse voltages. *E*: the number of spikes evoked per electrical or optical stimulus pulse across the range of frequencies tested during repetitive stimulation. *F*: when the number of spikes evoked per stimulus pulse was plotted against stimulus frequency, optical but not electrical stimulation showed a significant reduction in spikes per pulse with increased frequency ($P = 0.0065$ and 0.4937, when compared with zero slope, respectively, $n =$ 15 and 12, optical and electrical stimulation, respectively). The slope of the two lines also differed significantly ($P = 0.0383$). This reflects the loss of stimulation efficacy with increased frequency of optical but not electrical stimulation. *G*: spike latency across different frequencies of repetitive optical and electrical stimulations. *H*: when spike latency (regression) was plotted against stimulus frequency, optical but not electrical stimulation showed a negative slope significantly different from zero ($P = 0.0457$ and 0.2410, respectively). There was no significant difference between the slopes of the two types of stimulation ($P = 0.1957$, $n = 15$ and 13, optical and electrical stimulation, respectively). Graphs show animal replicates and/or means ± SE. ChR2, channelrhodopsin; EMG, electromyography; VMR, visceromotor response.

four stimulation-quiescence cycles. A significant increase in the duration of abdominal grooming, but not the number of episodes, was detected with phasic stimulation [$P = 0.039$, Dunn's posttest (stimulation vs. prestimulation control period), repeated measures Friedman test, Friedman statistic = 8.1, $P = 0.044$, $n = 7$, rectal stimulation group; Supplemental Fig. S3]. No change in ear, back, or nose grooming was recorded (Supplemental Fig. S3). Taken together, these findings suggest that continuous trains of action potentials along rectal-projecting afferents were more effective for inducing self-grooming motor sequences. To our surprise, no writhing or prominent abdominal contractions were detected following continuous or phasic stimulation of rectal stimulation of the gut-brain axis ($n =$ 10, see Supplemental Video S1).

The limited increases in VMR responses to higher frequency optical stimulations suggested behavioral responses to in vivo stimulation may be similar at stimulation frequencies lower than 20 Hz. Additional behavioral experiments using the continuous rectal stimulation protocol at 1 Hz (1% duty cycle, 10 W power; $n = 4$) and 20 Hz in the same mice (20% duty cycle, 10 W power; $n = 4$) revealed little difference between the two stimulation frequencies (Supplemental Fig. S4). Additional experiments revealed only 20 Hz stimulations significantly reduced movement [$P = 0.018$, Dunnett's posttest, two-way ANOVA, main effect of stimulation frequency $P = 0.145$, $F(1.00, 6.00) = 2.8$, $n = 7$ and 4, 20 Hz and 1 Hz, respectively; Supplemental Fig. S4].

Wireless Optogenetic Stimulation of the Peritoneal Cavity

We next sought to investigate whether similar behavioral responses were elicited by identical light stimuli applied to the inner wall of the peritoneal cavity—a region anatomically distinct from the gut-brain axis. Here, the LEDs were facing the abdominal wall away from the colon/rectum tissue. When the continuous stimulation protocol was delivered to conscious, untethered Trpv1^{Cre+}ChR2 mice, robust contraction

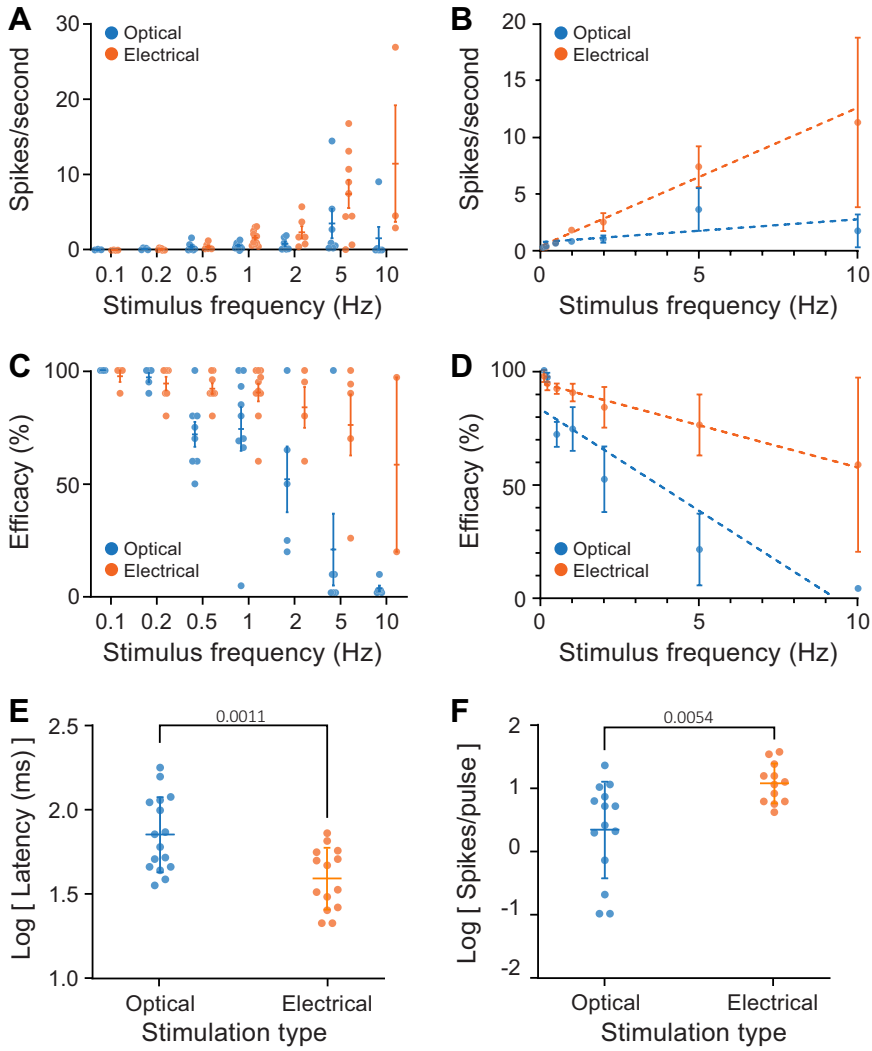

Figure 5. Number of muscle action potentials evoked by hard-wired LED stimulation in anesthetized Trpv1^{Cre+}ChR2 mice. *A* and *B*: when the number of evoked spikes was plotted against stimulus, the slope of electrical but not optical stimulation was significantly different from zero ($P < 0.001$, $n = 15$ total; optical stimulation = 15, electrical stimulation = 12). The slopes of electrical and optical stimulation were significantly different ($P < 0.001$). Thus, while optical stimulation evoked a relatively constant number of spikes across increasing stimulation frequencies and durations, the spikes evoked by electrical stimulation continued to increase. This is explicable by the greater loss of optical stimulation efficacy with increasing frequency compared with electrical stimulation. *C* and *D*: when stimulation efficacy was plotted against stimulation frequency, both optical but not electrical stimulation showed a negative slope, significantly different from zero ($P < 0.001$ and = 0.769, respectively, $n = 15$ total; optical stimulation = 15, electrical stimulation = 12). The negative slope of the optical stimulation was significantly different from electrical stimulation ($P < 0.001$). Thus, the rate of loss of stimulation efficacy with increased frequency was greater for optical stimulation, compared with electrical stimulation. *E*: spike latency, the time between suprathreshold stimuli and muscle action potentials, was consistently less for electrical stimulation compared to optical stimulation ($P = 0.001$, paired *t* test, $t = 4.256$, df = 12, $n = 13$). This may reflect the additional recruitment of faster-conducting fibers by electrical stimulation. *F*: the number of spikes within bursts of firing that regularly followed stimulation was quantified. Electrical stimulation always evoked more spikes than optical stimulation ($P = 0.005$, paired *t* test, $t = 3.539$, df = 10, $n = 11$). Graphs show animal replicates and/or means ± SE. ChR2, channelrhodopsin; LED, light-emitting diode.

of the abdominal musculature (see yellow arrows in Fig. 6*D*) and an increase in the number of writhing events were readily observed (Fig. 6, *D* and *E*, and Supplemental Video S1). These are indicated by the red arrow showing leg extension in Fig. 6*D*. Writhing was never observed during the prestimulation baseline periods or in the other groups of mice (rectal stimulation and surgical control; Fig. 6*E*). Continuous peritoneal stimulation also induced a significant increase in abdominal grooming episodes [prestimulation: 0.0 ± 0.0; during stimulation: 2.5 ± 1.3; $P = 0.019$, Dunn's posttest (stimulation vs. prestimulation control period), repeated measures Friedman test, Friedman statistic = 9.00, $P = 0.008$, $n = 6$, peritoneal stimulation group] and the duration of abdominal grooming compared with the prestimulation period [prestimulation: 0.0 ± 0.0 s; during stimulation: 4.2 ± 3.3; $P = 0.042$, Dunn's posttest (stimulation vs. prestimulation control period), repeated measures Friedman test, Friedman statistic = 9.33, $P = 0.005$, $n = 6$, peritoneal stimulation group]. These results are shown graphically in Fig. 6, *B* and *C*. An example of abdominal grooming associated with optogenetic stimulation of the peritoneum in a Trpv1^{Cre+}ChR2 mouse is shown in Fig. 6*A*. Unlike rectal stimulation, stimulation of the peritoneum did not significantly change total voluntary movement around the cavity (Fig. 7, *A* and *B*). Similar to rectal stimulations, the stimulation of the peritoneum did not significantly affect the occurrence of grooming behavior of the back, nose, and ears (Fig. 7, *C–E*). No significant change in voluntary movement was observed in the control group (Fig. 7, *B–F*). When the phasic stimulation protocol was applied to the peritoneal cavity, no significant changes were detected in abdominal, nose, back, or ear grooming ($n = 6$, Supplemental Fig. S3). Again, these findings suggest a continuous train of action potentials in gut-brain afferents innervating the distal colon/rectum was more effective for inducing the grooming phenotype. Following in vivo experimentation, the integrity of the colon was assessed. No significant difference in the histology of rectum tissues was identified across all experimental groups (Supplemental Fig. S5).

DISCUSSION

The findings of the current study show that distinct behavior responses can be induced in response to highly controlled optogenetic stimulation of the gut-brain axis in conscious freely moving mice, using wireless, fully implantable custom-made battery-free devices. Understanding how

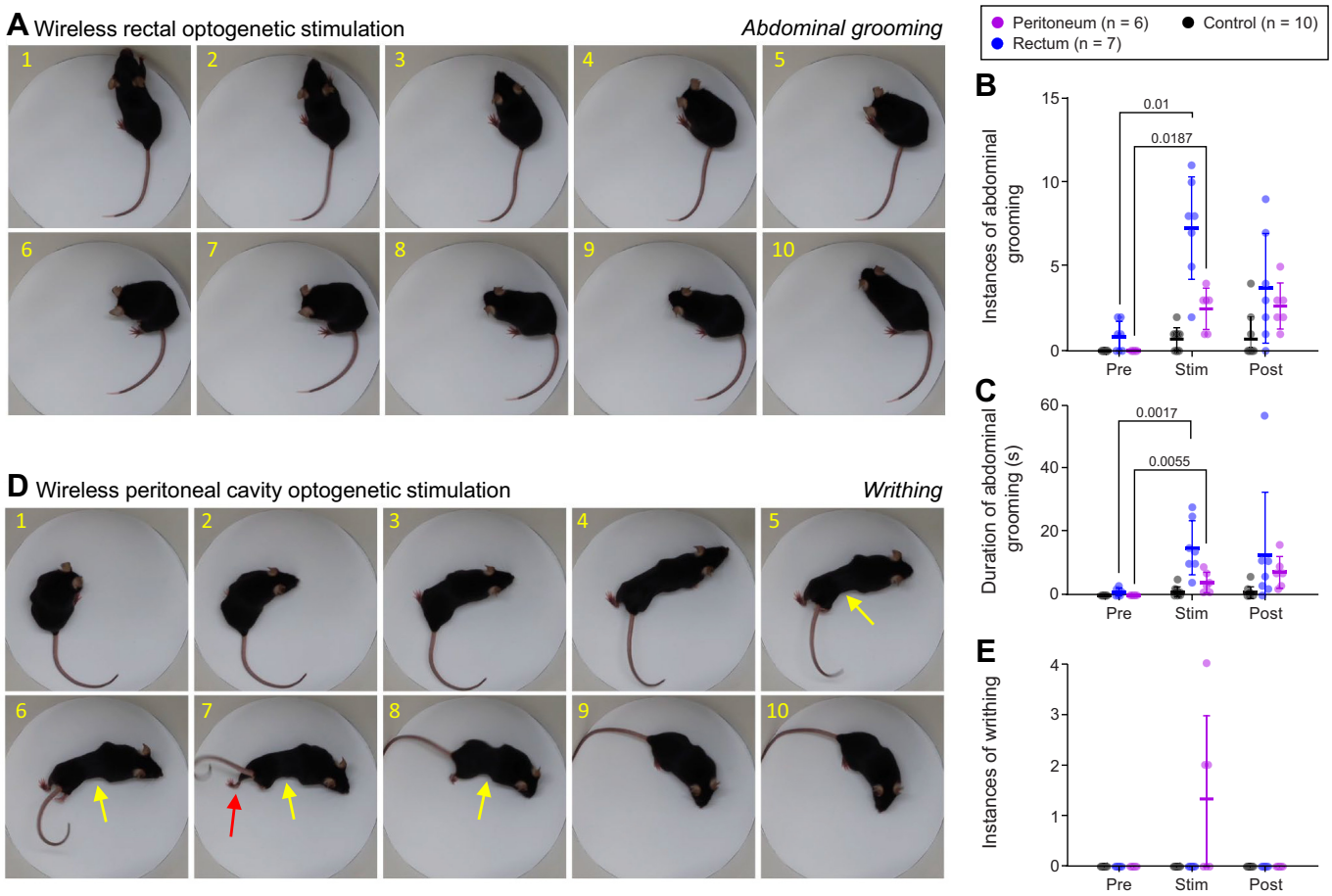

Figure 6. Behavioral effects of wireless optogenetic stimulation of the rectum in conscious untethered Trpv1^{Cre+}ChR2 mice. *A*: stimulation evoked increased bouts of abdominal grooming, as shown in this sequence of images from *1* to *10*. *B*: graph showing significant increase in instances of abdominal grooming during stimulation using devices implanted in the rectum, or peritoneal cavity. *C*: graph showing significant increase in the duration of grooming events when the wireless device delivered optical stimulation to the rectum and peritoneal cavity. *D*: wireless optogenetic stimulation of the peritoneal cavity induced writhing, characterized by hind leg extension (see red arrow in *7*) and robust contraction of the abdominal muscles (a viscero-motor response, see yellow arrow). *E*: graph showing increases in writhing when peritoneal stimulation is applied, but not via rectal stimulation. Graphs show animal replicates and means ± SD. ChR2, channelrhodopsin.

different regions along the gut-brain axis contribute to behavior in conscious freely moving animals is a significant technical challenge. We used a miniature implanted device that relies on wireless power transfer to provide highly targeted optogenetic stimulation of the distal colon and rectum in untethered mice (23). The distal colon/rectum was selected for optogenetic stimulation because the device can be implanted and adheres reliably to the terminal gut to provide controlled optogenetic stimulation. This region of the gut is densely innervated by spinal afferent endings, but we were unable to identify vagal afferent axons or endings in the distal region, using our methods, which was the region where optogenetic stimulation was delivered (26). The most likely explanation for the behavioral changes induced by optogenetic stimulation from the distal colon/rectal region is the activation of spinal afferents. However, we cannot rule out the possibility that a small population of vagal afferents reach the site of optogenetic stimulation. Indeed, other sensory and motor nerve pathways innervate the distal region of the mouse large intestine. This includes intestinofugal neurons, sympathetic and parasympathetic axons. How these axons could be activated by blue light delivered via wireless devices is unclear.

In a recent wireless optogenetic device development, a flexible multifunctional probe directly implants inside the intestinal lumen, whereas the wireless receiver lay exteriorized and affixed on the skull of mice (28). In contrast, in this study, we mounted the LED array outside the gut wall, whereas the wireless receiver was fully implanted inside the animal. This configuration allowed direct optogenetic stimulation of the extrinsic axons that underlie the gut-brain axis, without reducing the intraluminal surface area that could limit gut content motility.

The major findings show that optogenetic stimulation of extrinsic afferents arising from the distal colon and rectum led to significant increases in the number of bouts of, and time spent during, abdominal grooming. Voluntary movements were significantly reduced during optogenetic stimulation. No changes were detected in nose/ear or back grooming with stimulation of the rectal spinal afferent stimulation. To our surprise, classic visceral pain behaviors like writhing and abdominal contractions were not detected by light activation of the axons of spinal afferents innervating

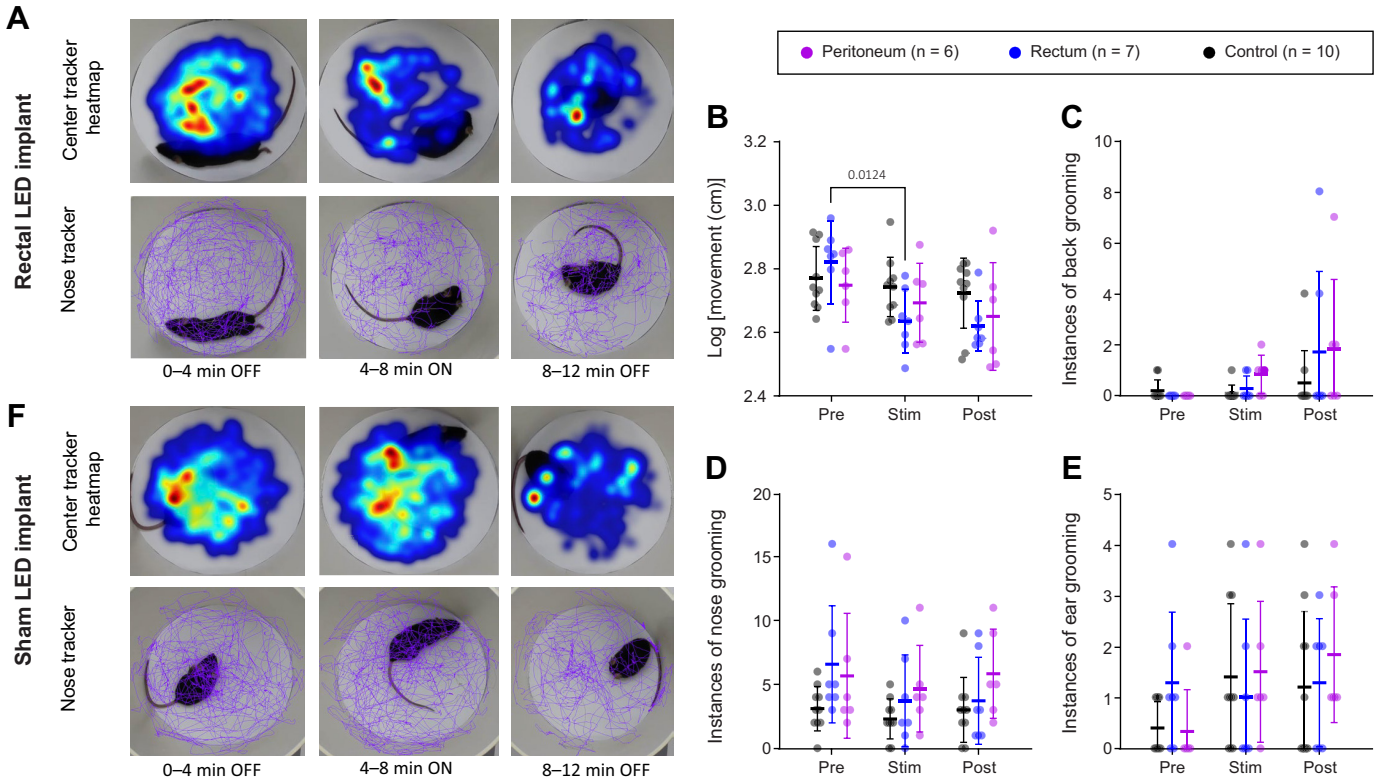

Figure 7. Locomotion in mice implanted with wireless devices. *A*: heat maps and traces showing movement trajectories of Trpv1^{Cre+}ChR2 mice in 4 min epochs before, during, and after stimulation. *B*: graph showing rectal but not peritoneal stimulation led to a significant reduction in voluntary movement, which remained low after stimulation. *C*: no changes in back grooming during stimulation. *D*: no changes in nose grooming. *E*: no changes in ear grooming. *F*: heat maps and trajectory traces showing voluntary movements in control mice. Graphs show animal replicates and means ± SD. ChR2, channelrhodopsin; LED, light-emitting diode.

the rectum. When the same stimulus parameters applied to the rectum were delivered to the peritoneal cavity, different behavioral responses were evoked (see Supplemental Video S1—Trpv1^{Cre+}ChR2 mice). Peritoneal stimulation (which would activate both visceral and somatic afferents) induced writhing and abdominal contractions (Fig. 6*D*). Instances of abdominal grooming and time spent grooming were significantly increased during stimulation, like rectal stimulation (Fig. 6, *B* and *C*).

When all optogenetic stimulation parameters remained constant, but a phasic rather than continuous pattern of illumination was applied to the peritoneal cavity or rectum, less behavioral changes were detected. That is, to elicit the increased grooming behavior from rectal stimulation, or writhing from the peritoneal stimulation, a continuous barrage of light pulses was more effective. Two geographically distinct populations of DRG neurons innervate the rectum, one in the thoracolumbar spinal segment; the other major population is in the lumbosacral spinal cord (6). It is not clear whether the anxiety-like phenotype we elicited by optogenetic stimulation of the rectum is due to activation of thoracolumbar or lumbosacral DRGs, or both populations of sensory neurons.

How the central nervous system processes different patterns of neuronal firing from the rectum differentially in Trpv1^{Cre+}ChR2 mice to elicit a grooming response instead of a classic writhing reflex from the rectum remains unclear. To minimize the number of variables, we maintained the frequency and light pulse constant but altered the stimulation from a continuous to phasic pattern. It should be noted that wireless stimulation in vivo was delivered onto the serosal surface, whereas in anesthetized mice, light was delivered onto the mucosal surface to elicit the classic visceromotor response. Based on the extensive spinal afferent innervation to the rectum and relative paucity of vagal afferents to this region, we expect that optogenetic stimulation would preferentially activate spinal afferents innervating the rectum to induce a classic abdominal contraction, writhing, and vocalization, commonly associated with visceral pain. It is apparent that many of spinal afferent axons to the rectum are activated at low thresholds, well below the threshold for eliciting nociceptive reflexes (6).

Using anterograde tracing from nodose ganglia, our findings revealed sparse labeling of vagal afferent axons and their endings in the proximal colon, with limited labeling in the mid colon. We were unable to identify any vagal afferent axons in the distal colon or rectum. These findings were supported by retrograde labeling from the distal colon using DiI. This suggests that the vagus nerve provides either a very limited sensory innervation or no sensory innervation to the distal colon and rectum of mice. This conclusion is supported by the work of other laboratories using transgenic Gpr65 or PhoX2B reporter mice, which are selective for vagal afferents (14). These studies showed extensive vagal afferent innervation in the upper gut, with very limited innervation in the colon. Our studies do not provide definitive proof that

there is no vagal afferent innervation to the distal gut of mice. It is possible that other anterograde tracers may fill some vagal afferent axons more comprehensively and label some axons in the distal colon and rectum. We have only performed anterograde tracing using dextran biotin, which provided comprehensive labeling in the upper gut when injected into nodose ganglia. It should be noted that we found many neurons were labeled in nodose ganglia after injecting CTB as a retrograde tracer into the distal gut of mice. This was conspicuously associated with extensive spread of tracer within the colon. This spread occurred even after single injections of very small volumes of tracer (~1 μL). Hence, relying on CTB via retrograde tracing to prove vagal afferents innervate the distal gut of mice should be interpreted with caution. In contrast to our findings reported here, recent studies from other laboratories have suggested that there is an extensive vagal afferent innervation to the distal colon of mice (29, 30). These studies used CTB as a retrograde tracer, injecting approximately five times greater volume into the colon wall than was used here, and these studies used large-diameter needles and multiple injections (puncture sites) into the gut wall.

Studies of the vagal afferent innervation of the rat colon are very similar to our results here in mouse, because the work of Wang and Powley showed a progressive decline in vagal afferent innervation along the length of the gut, with no apparent labeling in the distal colon as seen in Fig. 20 of Ref. 8. Studies have shown different transport times for DiI between the gut and DRG compared with nodose ganglia (7). These differences in transport time are unlikely to explain our extensive labeling of DRG, but not in nodose ganglia, because data from transgenic mice selectively labeling vagal afferents (14) match well with our results from anterograde tracing from nodose ganglia.

Implantable, wireless battery-free optogenetic stimulators, strategically designed to interface with soft tissues, represent a technological advantage that enables the study of the intricate gut-brain circuit in freely behaving mice. Using such a technology, we reveal that light activation of a localized population of extrinsic axons within the gut-brain axis from the terminal rectum elicits increased grooming phenotype in conscious untethered mice. The findings suggest that wireless optogenetic technology can be used to interrogate the functional role of targeted regions along the gut-brain axis in freely moving animals.

DATA AVAILABILITY

All data generated or analyzed during this study are included in the article and supporting files. Any additional information required to reanalyze the data reported in this paper is available upon request.

SUPPLEMENTAL MATERIAL

Supplemental Figs. S1–S5 and Supplemental Video S1: https://doi.org/10.5281/zenodo.13932344.

ACKNOWLEDGMENTS

The authors acknowledge the facilities of Microscopy Australia and the Australian National Collaborative Research Infrastructure Strategy, at the South Australian Regional Facility, Flinders Microscopy and Microanalysis, Flinders University.

GRANTS

This work was supported by National Health and Medical Research Council (NHMRC) Project Grant no. 1156427 and an Australian Research Council (ARC) Discovery Project Grant no. DP220100070; the Querrey-Simpson Institute for Bioelectronics; and the start-up fund from North Carolina State University, Grant no. 201473-02139.

DISCLOSURES

No conflicts of interest, financial or otherwise, are declared by the authors.

AUTHOR CONTRIBUTIONS

T.J.H., L.T., H.H., J.A.R., N.J.S., and A.V.-G. conceived and designed research; T.J.H., A.E., Y.W., L.T., K.T., M.-K.L., J. Kim, J. Kang, M.R., M.K., and V.Z. performed experiments; T.J.H., L.T., K.T., and N.J.S. analyzed data; T.J.H., A.E., M.W., L.T., H.H., J.A.R., and N.J.S. interpreted results of experiments; T.J.H., M.W., and A.V.-G. prepared figures; T.J.H. and N.J.S. drafted manuscript; T.J.H., M.W., L.T., J.A.R., N.J.S., and A.V.-G. edited and revised manuscript; and J.A.R., N.J.S., and A.V.-G. approved final version of manuscript.

REFERENCES

1. **Margolis KG**, **Cryan JF**, **Mayer EA.** The microbiota-gut-brain axis: from motility to mood. *Gastroenterology* 160: 1486–1501, 2021. doi:10.1053/j.gastro.2020.10.066.
2. **Labanski A**, **Langhorst J**, **Engler H**, **Elsenbruch S.** Stress and the brain-gut axis in functional and chronic-inflammatory gastrointestinal diseases: a transdisciplinary challenge. *Psychoneuroendocrinology* 111: 104501, 2020. doi:10.1016/j.psyneuen.2019.104501.
3. **Fairbrass KM**, **Lovatt J**, **Barberio B**, **Yuan Y**, **Gracie DJ**, **Ford AC.** Bidirectional brain-gut axis effects influence mood and prognosis in IBD: a systematic review and meta-analysis. *Gut* 71: 1773–1780, 2022. doi:10.1136/gutjnl-2021-325985.
4. **Gebhart GF**, **Bielefeldt K.** Physiology of visceral pain. *Compr Physiol* 6: 1609–1633, 2016. doi:10.1002/cphy.c150049.
5. **Brookes SJ**, **Spencer NJ**, **Costa M**, **Zagorodnyuk VP.** Extrinsic primary afferent signalling in the gut. *Nat Rev Gastroenterol Hepatol* 10: 286–296, 2013. doi:10.1038/nrgastro.2013.29.
6. **Brierley SM**, **Hibberd TJ**, **Spencer NJ.** Spinal afferent innervation of the colon and rectum. *Front Cell Neurosci* 12: 467, 2018. doi:10.3389/fncel.2018.00467.
7. **Ma J**, **Nguyen D**, **Madas J**, **Bizanti A**, **Mistareehi A**, **Kwiat AM**, **Chen J**, **Lin M**, **Christie R**, **Hunter P**, **Heal M**, **Baldwin S**, **Tappan S**, **Furness JB**, **Powley TL**, **Cheng ZJ.** Organization and morphology of calcitonin gene-related peptide-immunoreactive axons in the whole mouse stomach. *J Comp Neurol* 531: 1608–1632, 2023. doi:10.1002/cne.25519.
8. **Wang FB**, **Powley TL.** Topographic inventories of vagal afferents in gastrointestinal muscle. *J Comp Neurol* 421: 302–324, 2000. doi:10.1002/(SICI)1096-9861(20000605)421:3<302::AID-CNE2>3.3.CO;2-E.
9. **Fox EA**, **Phillips RJ**, **Baronowsky EA**, **Byerly MS**, **Jones S**, **Powley TL.** Neurotrophin-4 deficient mice have a loss of vagal intraganglionic mechanoreceptors from the small intestine and a disruption of short-term satiety. *J Neurosci* 21: 8602–8615, 2001. doi:10.1523/JNEUROSCI.21-21-08602.2001.
10. **Altschuler SM**, **Escardo J**, **Lynn RB**, **Miselis RR.** The central organization of the vagus nerve innervating the colon of the rat. *Gastroenterology* 104: 502–509, 1993. doi:10.1016/0016-5085(93)90419-d.
11. **Sengupta JN.** Visceral pain: the neurophysiological mechanism. *Handb Exp Pharmacol* 194: 31–74, 2009. doi:10.1007/978-3-540-79090-7_2.

12. **Berthoud HR**, **Neuhuber WL.** Functional and chemical anatomy of the afferent vagal system. *Auton Neurosci* 85: 1–17, 2000. doi:10.1016/S1566-0702(00)00215-0.
13. **Ness TJ**, **Gebhart GF.** Colorectal distension as a noxious visceral stimulus: physiologic and pharmacologic characterization of pseudaffective reflexes in the rat. *Brain Res* 450: 153–169, 1988. doi:10.1016/0006-8993(88)91555-7.
14. **Borgmann D**, **Ciglieri E**, **Biglari N**, **Brandt C**, **Cremer AL**, **Backes H**, **Tittgemeyer M**, **Wunderlich FT**, **Brüning JC**, **Fenselau H.** Gut-brain communication by distinct sensory neurons differently controls feeding and glucose metabolism. *Cell Metab* 33: 1466–1482.e7, 2021. doi:10.1016/j.cmet.2021.05.002.
15. **Goldstein N**, **McKnight AD**, **Carty JRE**, **Arnold M**, **Betley JN**, **Alhadeff AL.** Hypothalamic detection of macronutrients via multiple gut-brain pathways. *Cell Metab* 33: 676–687.e5, 2021. doi:10.1016/j.cmet.2020.12.018.
16. **Bayrer JR**, **Castro J**, **Venkataraman A**, **Touhara KK**, **Rossen ND**, **Morrie RD**, **Maddern J**, **Hendry A**, **Braverman KN**, **Garcia-Caraballo S**, **Schober G**, **Brizuela M**, **Castro Navarro FM**, **Bueno-Silva C**, **Ingraham HA**, **Brierley SM**, **Julius D.** Gut enterochromaffin cells drive visceral pain and anxiety. *Nature* 616: 137–142, 2023. doi:10.1038/s41586-023-05829-8.
17. **Kyloh M**, **Nicholas S**, **Zagorodnyuk VP**, **Brookes SJ**, **Spencer NJ.** Identification of the visceral pain pathway activated by noxious colorectal distension in mice. *Front Neurosci* 5: 16, 2011. doi:10.3389/fnins.2011.00016.
18. **Zhang S**, **Chen L**, **Feng B.** An anesthesia protocol for robust and repeatable measurement of behavioral visceromotor responses to colorectal distension in mice. *Front Pain Res (Lausanne)* 4: 1202590, 2023. doi:10.3389/fpain.2023.1202590.
19. **Morteau O**, **Hachet T**, **Caussette M**, **Bueno L.** Experimental colitis alters visceromotor response to colorectal distension in awake rats. *Dig Dis Sci* 39: 1239–1248, 1994. doi:10.1007/BF02093789.
20. **Coutinho SV**, **Meller ST**, **Gebhart GF.** Intracolonic zymosan produces visceral hyperalgesia in the rat that is mediated by spinal NMDA and non-NMDA receptors. *Brain Res* 736: 7–15, 1996. doi:10.1016/0006-8993(96)00661-0.
21. **Jones RC III**, **Gebhart GF.** Models of visceral pain: colorectal distension (CRD). *Curr Protoc Pharmacol* 25: 5.36.1–5.36.17, 2004. doi:10.1002/0471141755.ph0536s25.
22. **Lindström E**, **Brusberg M**, **Hughes PA**, **Martin CM**, **Brierley SM**, **Phillis BD**, **Martinsson R**, **Abrahamsson C**, **Larsson H**, **Martinez V**, **Blackshaw AL.** Involvement of metabotropic glutamate 5 receptor in visceral pain. *Pain* 137: 295–305, 2008. doi:10.1016/j.pain.2007.09.008.
23. **Efimov AI**, **Hibberd TJ**, **Wang Y**, **Wu M**, **Zhang K**, **Ting K**, **Madhvapathy S**, **Lee MK**, **Kim J**, **Kang J**, **Riahi M**, **Zhang H**, **Travis L**, **Govier EJ**, **Yang L**, **Kelly N**, **Huang Y**, **Vázquez-Guardado A**, **Spencer NJ**, **Rogers JA.** Remote optogenetic control of the enteric nervous system and brain-gut axis in freely-behaving mice enabled by a wireless, battery-free optoelectronic device. *Biosens Bioelectron* 258: 116298, 2024. doi:10.1016/j.bios.2024.116298.
24. **Yang Y**, **Wu M**, **Vázquez-Guardado A**, **Wegener AJ**, **Grajales-Reyes JG**, **Deng Y**, **Wang T**, **Avila R**, **Moreno JA**, **Minkowicz S**, **Dumrongprechachan V**, **Lee J**, **Zhang S**, **Legaria AA**, **Ma Y**, **Mehta S**, **Franklin D**, **Hartman L**, **Bai W**, **Han M**, **Zhao H**, **Lu W**, **Yu Y**, **Sheng X**, **Banks A**, **Yu X**, **Donaldson ZR**, **Gereau RW 4th**, **Good CH**, **Xie Z**, **Huang Y**, **Kozorovitskiy Y**, **Rogers JA.** Wireless multilateral devices for optogenetic studies of individual and social behaviors. *Nat Neurosci* 24: 1035–1045, 2021 [Erratum in *Nat Neurosci* 25: 1394, 2022]. doi:10.1038/s41593-021-00849-x.
25. **Yang Y**, **Wu M**, **Wegener AJ**, **Vázquez-Guardado A**, **Efimov AI**, **Lie F**, **Wang T**, **Ma Y**, **Banks A**, **Li Z**, **Xie Z**, **Huang Y**, **Good CH**, **Kozorovitskiy Y**, **Rogers JA.** Preparation and use of wireless reprogrammable multilateral optogenetic devices for behavioral neuroscience. *Nat Protoc* 17: 1073–1096, 2022. doi:10.1038/s41596-021-00672-5.
26. **Spencer NJ**, **Kyloh M**, **Duffield M.** Identification of different types of spinal afferent nerve endings that encode noxious and innocuous stimuli in the large intestine using a novel anterograde tracing technique. *PLoS One* 9: e112466, 2014. doi:10.1371/journal.pone.0112466.
27. **Ausra J**, **Wu M**, **Zhang X**, **Vázquez-Guardado A**, **Skelton P**, **Peralta R**, **Avila R**, **Murickan T**, **Haney CR**, **Huang Y**, **Rogers JA**, **Kozorovitskiy Y**, **Gutruf P.** Wireless, battery-free, subdermally implantable platforms for transcranial and long-range optogenetics in freely moving animals. *Proc Natl Acad Sci USA* 118: e2025775118, 2021. doi:10.1073/pnas.2025775118.
28. **Sahasrabudhe A**, **Rupprecht LE**, **Orguc S**, **Khudiyev T**, **Tanaka T**, **Sands J**, **Zhu W**, **Tabet A**, **Manthey M**, **Allen H**, **Loke G**, **Antonini MJ**, **Rosenfeld D**, **Park J**, **Garwood IC**, **Yan W**, **Niroui F**, **Fink Y**, **Chandrakasan A**, **Bohórquez DV**, **Anikeeva P.** Multifunctional microelectronic fibers enable wireless modulation of gut and brain neural circuits. *Nat Biotechnol* 42: 892–904, 2024. doi:10.1038/s41587-023-01833-5.
29. **Osman S**, **Tashtush A**, **Reed DE**, **Lomax AE.** Analysis of the spinal and vagal afferent innervation of the mouse colon using neuronal retrograde tracers. *Cell Tissue Res* 392: 659–670, 2023. doi:10.1007/s00441-023-03769-3.
30. **Wang Q**, **Caraballo SG**, **Rychkov G**, **McGovern AE**, **Mazzone SB**, **Brierley SM**, **Harrington AM.** Comparative localization of colorectal sensory afferent central projections in the mouse spinal cord dorsal horn and caudal medulla dorsal vagal complex. *J Comp Neurol* 532: e25546, 2024. doi:10.1002/cne.25546.